Mitigation and Adaptation Strategies for Global Change
https://doi.org/10.1007/s11027-019-09865-6

ORIGINAL ARTICLE

Evapotranspiration in North America: implications for water resources in a changing climate

Yang Qu [1,2] · Qianlai Zhuang [1,3]

Received: 24 January 2019 / Accepted: 25 April 2019/Published online: 15 May 2019

Abstract

Accurate quantification of evapotranspiration (ET) is important to understanding its role in the global hydrological cycle of terrestrial ecosystems and feedbacks to the climate system. This study improves ET quantification in North America using a data assimilation technique and a process-based Terrestrial Ecosystem Model as well as in situ and satellite data. ET is modeled using the Penman-Monteith equation with an improved leaf area index (LAI) algorithm in a biogeochemistry model, the Terrestrial Ecosystem Model (TEM). The evaluated TEM was used to estimate ET at site and regional scales in North America from 2000 to 2010. The estimated annual ET varies from 420 to 450 mm year^{-1} with the improved model, close to Moderate Resolution Imaging Spectroradiometer monthly data with a root-mean-square error less than 10 mm month^{-1} for the study period. Alaska, Canada, and the conterminous US account for 33%, 6%, and 61% of the regional ET, respectively. Water availability, the difference between precipitation and ET, is 181 mm month^{-1}, averaged from 2000 to 2010. Under IPCC Representative Concentration Pathway (RCP) 2.6 and RCP 8.5 scenarios, the regional ET increases by 11% and 24%, respectively. Consequently, the water availability decreases in the region by 2.4% and 23.7%, respectively. For the period of 2020–2100, due to uncertain parameters, TEM versions integrated with three different ET algorithms estimated that the regional ET in the USA are 430.5 ± 10.5 mm year^{-1}, 482.1 ± 11.2 mm year^{-1}, and 489.7 ± 13.4 mm year^{-1}, and the available water is -105.3 ± 8.7 mm year^{-1}, -20.3 ± 11.9 mm year^{-1}, and -126.2 ± 15.4 mm year^{-1}, respectively, by the end of the twenty-first century. Our analysis suggests natural terrestrial ecosystem soils in North America will get drier under future climate conditions, which will impact the regional water resource and the climate system. Based on our ET simulation under three climate change scenarios, our study suggests that the RCP 2.6 is the optimum trajectory for preserving freshwater resources in North America and other regions in the globe.

Keywords Evapotranspiration · Terrestrial ecosystem model · Water resource · Climate change

✉ Qianlai Zhuang
qzhuang@purdue.edu

Extended author information available on the last page of the article

1 Introduction

Evapotranspiration (ET) is an important water flux in the terrestrial ecosystem hydrological cycle (Dolman and De Jeu 2010) and is also a key energy flux of the land surface. ET links the atmosphere and ecosphere through the energy exchange and biogeochemical cycles (Betts et al. 1996; Mu et al. 2007; Sun et al. 2011; Katul et al. 2012). Different models showed that 60–67% of annual precipitation returns as ET to the atmosphere (Vörösmarty et al. 1998; Miralles et al. 2011; Zhang et al. 2016). The response of ET to increasing temperature and greenhouse gas concentrations will impact the climate system and water availability to the human system. Accurate quantification of ET is important to estimating regional water balance and water availability, an important ecosystem service (Mooney et al. 2005), and to conducting economic analysis (Vörösmarty et al. 2010).

Recent studies have been continuously developing process-based ecosystem and hydrological models that simulate the essential physical interactions between ecosystem ET and changing climate. For instance, hydrological models (Vörösmarty et al. 1998), dynamic vegetation models (Sitch et al. 2003), land surface models (Liang et al. 1994), and other simple models designed to use satellite Earth observations as input (Mueller et al. 2013) have been used for ET quantification. These numerical models have the ability to project ET at global scales under different climate conditions at various spatial and temporal resolutions.

To adequately quantify regional ET across space and time, terrestrial ecosystem models with well-constrained parameters using observed data are needed. Currently, ET quantification is still of large uncertainties due to uncertain forcing data and inadequate representation of the physical processes in the models (Liu et al. 2015). The uncertainties come from different environmental factors including plant phenology, soil moisture, solar radiation, temperature, and wind speed. The uncertainty of previous quantification of ET at regional scales may also come from using a limited amount of in situ data of ET for model parameterization and verification (e.g., Liu et al. 2014). However, in recent decades, satellite and remote sensing have provided continuous ET data at both high spatial and temporal resolutions at the global scale (Allen et al. 2005), which shall help improve regional quantification. For instance, Moderate Resolution Imaging Spectroradiometer (MODIS) ET (Mu et al. 2007) is available from 2000 to 2010 at a spatial resolution of 1 km and 8-day time resolution. This product was estimated using the improved ET algorithm (Mu et al. 2011) based on the Penman-Monteith equation (Monteith 1965). Global Potential Evapo-Transpiration (Global-PET) dataset (Zomer et al. 2008) is another high-resolution (30 arc s, about 1 km at the equator) global dataset, which was developed by combining four different algorithms including FAO application, Thornthwaite (1948), Thornthwaite modified by Holland (1978), and Hargreaves et al. (1985). Different methods of calculating ET have been tested for different regions (Liu et al. 2014; Lu and Zhuang 2010).

Plant transpiration (T), an important component of ET, is highly dependent on plant phenology, an indicator of seasonal variations of ecosystems (Edwards and Richardson 2004). Plant phenology as a periodical feature of global vegetation dynamics can be studied using vegetation indices (Zhang et al. 2003). The timing of start and end of vegetation growing is an important depiction of phenology. Therefore, satellite-based vegetation indices (VIs) have been used to characterize phenology (Asrar et al. 1989; Baret and Guyot 1991). Leaf area index (LAI) as a VI is important to modeling ET and photosynthesis (Duchemin et al. 2006; Wiegand et al. 1979). For instance, the Penman-Monteith ET is modeled as a function of LAI (Allen 2000).

Some studies have used simple approaches to estimate ET, such as by linking ET and remote sensing indices directly (Sobrino et al. 2005; Wang et al. 2007) and by using empirical functions to upscale site measurements to a region (Hargreaves and Allen 2003). The uncertainties from these existing studies are still large.

North America is a critical region for Earth's climate (Rasmusson 1968; Biederman et al. 2016). The region is sensitive to climate change and feedbacks significantly to the global climate system (Intergovernmental Panel on Climate Change 2014). It extends within 10° of latitude of both the equator and the North Pole and embraces every climatic zone from tropical rain forest and savanna on the lowlands of the Central America to areas of permanent ice cap in central Greenland. Subarctic and tundra climates prevail in north Canada and Alaska, and desert and semiarid conditions are found in interior regions cut off by high mountains from rain-bearing westerly winds. A large proportion of the continent has temperate climates, which are very favorable to settlement and agriculture. Accurate simulation of ET in North America under different climate change scenarios can improve our estimates of water balance responses to climate changes, which will help stakeholders to develop adaptation strategies in the twenty-first century and to mitigate the negative impacts of decreasing freshwater availability.

Previous studies focusing on evapotranspiration in North America have indicated that ET is sensitive to surface (e.g., plant canopy) conductance (Wilson and Baldocchi 2000). Therefore, it is possible to integrate the LAI model (Qu and Zhuang, 2018; Qu et al., 2018) into existing ecosystem models, such as the Terrestrial Ecosystem Model (TEM; Zhuang et al. 2003, 2010), to quantify ET. This study takes advantage of the existing ET data to verify an ecosystem model simulation of ET before applying the model to the region. The ET algorithms were revised to estimate monthly ET and water availability, defined as the difference between precipitation and ET. The revised ET improves the water balance model (WBM; Vörösmarty et al. 1998) to estimate soil moisture. To test this, high-resolution soil moisture satellite data of National Aeronatics and Space Administration Soil Moisture Active Passive (SMAP) are used to evaluate the model. In addition, three different algorithms of ET estimates were also adopted into an ecosystem model and were evaluated. The revised model is finally used to investigate the ET response to climate change from 2000 to 2010 and in the twenty-first century for the North America. Water availability and ET for the historical period and the twenty-first century is further evaluated in the context of water availability to the region and climatic impacts.

2 Method

2.1 Data

To quantify ET in North America, National Centers for Environmental Prediction (NCEP) global monthly climate data for the period 1985–2010 at a spatial resolution of 0.5° × 0.5° including precipitation, air temperature, and cloudiness are used. In addition, data of soil texture, elevation, and plant function types (PFTs) at the same spatial resolution are also used (Zhuang et al. 2003). MODIS monthly ET product from 2000 to 2010 at a spatial resolution of 0.5° × 0.5° is used to verify an ET model (Mu et al. 2007). To evaluate the revised TEM performance in estimating soil moisture, high-resolution soil moisture satellite data of NASA SMAP provided by Alaska Satellite Facility (ASF) and National Snow and Ice Data Center (NSIDC) is used. Specifically, the level 4 soil moisture data at soil surface and root zone at a 9-km resolution and every 7-day time step are used.

Future climate scenarios from 2016 to 2100 were generated under representative concentration pathways (RCPs), within Coupled Model Intercomparison Project Phase 5 (CMIP5). Here, we use the RCP 2.6 (Van Vuuren et al. 2007) and RCP 8.5 (Riahi et al. 2007) as two extreme case scenarios to examine changes in ET and water availability during the twenty-first century.

2.2 Model modification

Previous simulation of ET with TEM is based on the following formulae of potential evapotranspiration (PET) (Jensen and Haise 1963):

$$\mathrm{PET} = [(0.014 \times (1.8 \times T) + 32) - 0.37] \times R_S \times 0.016742 \times \mathrm{MD} \tag{1}$$

where T is the monthly average air temperature (°C), and R_S is the mean monthly shortwave radiation on top of the canopy (Cal cm^{-2} day^{-1}) calculated in TEM based on latitude, date, and cloudiness (Pan et al. 1996). MD is the number of days per month. This PET algorithm lacks the consideration of net outgoing longwave radiation and the aerodynamic aspects of ET on the atmospheric demand for water vapor. Therefore, PET estimated from the equation tends to underestimate ET in spring and overestimate ET in summer.

In this study, we revised the actual ET algorithm by integrating the effects of LAI into the Penman-Monteith (P-M) equation (Monteith 1965; Allen et al. 1998) in addition to considering the effects of radiation and temperature effects

$$\lambda \mathrm{ET} = \frac{\Delta \cdot (R_n - G) + \rho_a \cdot c_p \cdot \dfrac{(e_s - e_a)}{r_a}}{\Delta + \gamma \cdot \left(1 + \dfrac{r_s}{r_a}\right)} \tag{2}$$

where r_s represents the surface resistance (s m^{-1}), which is closely related to LAI and is modeled in Qu and Zhuang (2018); r_a is the aerodynamic resistance (s m^{-1}); Δ is the derivative of the saturation water vapor to temperature; $R_n - G$ is the available energy; $e_s - e_a$ is the water vapor pressure deficit (VPD); and r_s is calculated as follows:

$$r_s = \frac{r_i}{\mathrm{LAI}_{\mathrm{active}}} \tag{3}$$

where r_i is the bulk stomatal resistance of the well-illuminated leaf, and $\mathrm{LAI}_{\mathrm{active}}$ is the active leaf area index (here, we use half of the improved LAI to represent), which reflects the ratio of sunlit leaf area to the soil surface. For other parameters, we use Eqs. (4)–(7)

$$r_a = \frac{208}{u_2} \tag{4}$$

where u_2 is the wind speed at height of 2 m.

The atmospheric pressure is computed as follows:

$$P = 101.3 \times \left(\frac{293 - 0.0065z}{293}\right)^{5.26} \tag{5}$$

where z is the elevation (m).

The saturated water vapor pressure is computed as follows:

$$e_s = 0.6108e^{\left(\frac{17.27T}{T+237.3}\right)} \tag{6}$$

where T is the temperature in degree Celsius.

The slope of vapor pressure is computed as follows:

$$\Delta = \frac{4098\left[0.6108e^{\frac{17.27T}{T+237.3}}\right]}{(T+237.3)^2} \tag{7}$$

To compute the net radiation in each grid cell, Eqs. (8)–(11) are used

$$R_n = R_{ns} - R_{nl} \tag{8}$$

where R_{ns} is the net shortwave radiation (W m^{-2}), and R_{nl} is the net longwave radiation (W m^{-2}).

The solar radiation is computed as follows:

$$R_s = \left(a_s + b_s \frac{n}{N}\right) R_a \tag{9}$$

where R_a is extraterrestrial radiation (W m^{-2}); a_s and b_s are the constant parameters that represent the amount of radiation reaching the earth, respectively; and $\frac{n}{N}$ is the relative sunshine duration

$$R_{ns} = 0.77R_s \tag{10}$$

where R_s is solar or shortwave radiation (W m^{-2}).

$$R_{nl} = \sigma T^4 (0.34 - 0.14\sqrt{e_a})\left(1.35\frac{R_s}{R_{so}} - 0.35\right) \tag{11}$$

where $\frac{R_s}{R_{so}}$ is the relative shortwave radiation, and σ is the Stefan-Boltzmann constant (5.67×10^{-8} Wm^{-2} K^{-4}).

2.3 Alternative ET algorithms

In order to compare our improved ET algorithm (hereafter referred to as AL-1) to others, we adopt the other two algorithms to quantify ET. One algorithm (hereafter referred to as AL-2) is based on the revised Penman-Monteith equation (Liu et al. 2013). By separating transpiration from vegetation canopy, AL-2 calculated ET in two parts from canopy and soil surface, separately

$$\mathrm{ET} = T_c + E_{soil} \tag{12}$$

where T_c is

$$T_c = \frac{\Delta A_c + \rho c_p (\mathrm{VPD})/r_a}{\lambda\left(s + \gamma\left(1 + \frac{r_s}{r_a}\right)\right)} \times \mathrm{sec2day} \times \mathrm{MD} \tag{13}$$

where E_{soil} is

$$E_{soil} = \frac{\Delta A_{soil} + \rho c_p (VPD)/r_{as}}{\lambda\left(s + \gamma\left(1 + \frac{r_{tot}}{r_{as}}\right)\right)} \times sec2day \times MD \times RH^{\frac{VPD}{\beta}} \quad (14)$$

where A_c (W m^{-2}) is the available energy in the vegetation canopy, A_{soil} (W m^{-2}) is the available energy in the soil, s is the slope of the saturation vapor pressure curve (Pa K^{-1}) and is the function of air temperature (kg m^{-3}), ρ is the air density, C_p (J kg^{-1} K^{-1}) is the specific heat capacity of air, VPD (Pa) is the vapor pressure deficit (i.e., the saturated air vapor pressure minus the actual air vapor pressure), r_a (s m^{-1}) is the aerodynamic resistance, r_s (s m^{-1}) is the surface resistance to transpiration from the plant canopy, r_{as} is the aerodynamic resistance at the soil surface, r_{tot} is the sum of r_{as} and surface resistance to evaporation, λ (J kg^{-1}) is the latent heat of vaporization, ρ (kg m^{-3}) is the air density, γ (Pa K^{-1}) is the psychometric constant, sec2day (s day^{-1}) is the number of seconds in a day, E_{soil_pot} is the potential evaporation from soils, f_{SM} is the proxy of soil water deficit used to constrain soil evaporation, RH is the relative humidity, and β is the relative sensitivity of RH to VPD (Fisher et al. 2008). In this method, transpiration from canopy and evaporation from soil are both calculated in a similar form as the P-M equation, but with different energy balance equations. ET calculated by AL-2 is then constrained by water balance in TEM.

Another algorithm (AL-3) for calculating ET is the revised algorithm from Mu et al. (2011) and Song et al. (2017). In this method, evaporation from soil, wet plant 12, and transpiration from plant are computed separately

$$\lambda ET = \lambda E_{soil} + \lambda E_{wet\_c} + \lambda E_{trans} \quad (15)$$

where E_{soil} is the evaporation from soil, E_{wet_c} is the transpiration from wet plant canopy surface, and E_{trans} is the transpiration from plant. In this method, evaporation from snow and water bodies is also added for more accurate quantification.

2.4 Model parameterization, verification, and regional simulation

Site-level parameterization for ET is conducted for different PFTs at the selected sites using observational data (Table 1). Using the Markov chain Monte Carlo (MCMC) method (Metropolis et al. 1953; Hastings 1970), 100,000 parameter sets are generated for every PFT. For regional simulations, an optimum set of parameters for each pixel is obtained (Chen et al. 2011). To calibrate the model with MODIS ET data, remote sensing data are organized to monthly and 0.5° × 0.5° resolution. Optimum parameters for each grid are used for ET simulations for the period 1985–2010 and future simulations. To use the satellite data of ET to parameterize the model, the MCMC technique is also used in a spatially explicit manner (Chen et al. 2011). The Metropolis-Hasting algorithm is used to generate random walk values with a proposed probability density and decide whether to accept or reject a value based on a specified acceptance ratio (Qu and Zhuang 2018). We sample 10,000 parameter combinations for each grid in our regional calibrations.

The parameterized model is applied to estimate regional ET at a spatial resolution of 0.5° × 0.5° from 2000 to 2010. We also conduct regional simulations with the previous version of TEM with the default parameterization in Zhuang et al. (2003). Both simulations are compared with the MODIS ET product (Mu et al. 2007). Site-level parameterization for ET under different RCP scenarios from 2016 to 2100 is also conducted.

Table 1 Key parameter values for representative ecosystem types

	Alpine tundra	Wet tundra	Boreal forest	Temperate coniferous forest	Temperate deciduous forest	Grassland	Xeric shrubland	Tropical forest
β (hPa)	2.0	2.0	1.5	1.6	1.3	2.1	2.2	2.5
SLA (m^2 g^{-1} C)	0.01	0.008	0.009	0.009	0.008	0.01	0.008	0.008
C_L (m/s)	0.005	0.004	0.003	0.002	0.004	0.005	0.005	0.002

β represents the relative sensitivity of soil moisture to vapor pressure deficit. C_L represents the mean potential stomata conductance

SLA specific leaf area

3 Results

3.1 Comparison between simulated and observed evapotranspiration

The simulated annual ET is in a good agreement with remote sensing data (Fig. 1). The comparison between MODIS and simulated annual ET with the revised TEM indicates that they have similar spatial distributions. The difference mainly exists in low-latitude areas (Fig. 2a). The root-mean-square error (RMSE) between simulated ET with previous TEM and MODIS ET tends to be larger than that between the revised TEM and MODIS data (Fig. 2b). The RMSE for the revised TEM is 10.2 mm $month^{-1}$ and larger than 50 mm $month^{-1}$ for the previous version. The spatial distribution of ET error between two versions of the model is similar, both showing large differences in the southwest part of North America and small differences in the northern and western areas of the region.

Regional ET in North America is computed by adding each area-weighted value for all grids. Overall, the annual average ET from 2000 to 2010 computed from the revised TEM agrees well with MODIS ET (RMSE less than 100 mm $year^{-1}$). The largest ET is found in the southeast part of North America with annual ET over 1000 mm, while most area in the east and north has ET around 200 mm per year. The spatial distribution of ET for land ecosystem types agrees well between simulations and MODIS data. Estimated ET ranges from 200 mm $year^{-1}$ for scrublands to 700 mm $year^{-1}$ for evergreen broadleaf forests.

ET in North America is generally low in winter due to low available energy, low temperature, and low surface conductance. ET across North America generally increases from north to south, and the revised TEM captures the magnitude of seasonal ET variation and spatial patterns of increasing from north to south in the region. The ET in the southwestern North America has a decreasing trend, which is comparable with previous projections (Seager et al. 2007). The ET in deciduous forest is 50% higher than ET in coniferous forest, which is consistent with findings for the western North America (Chapin et al. 2000).

The revised TEM estimated that average ET in North America is 460 mm $year^{-1}$ during 2000–2010, lower than the MODIS ET of 483 mm $year^{-1}$. The spatial distribution of modeled ET matches well with satellite data ($R^2 = 0.78$), and the RMSE of monthly ET is small as 8.7 mm $month^{-1}$.

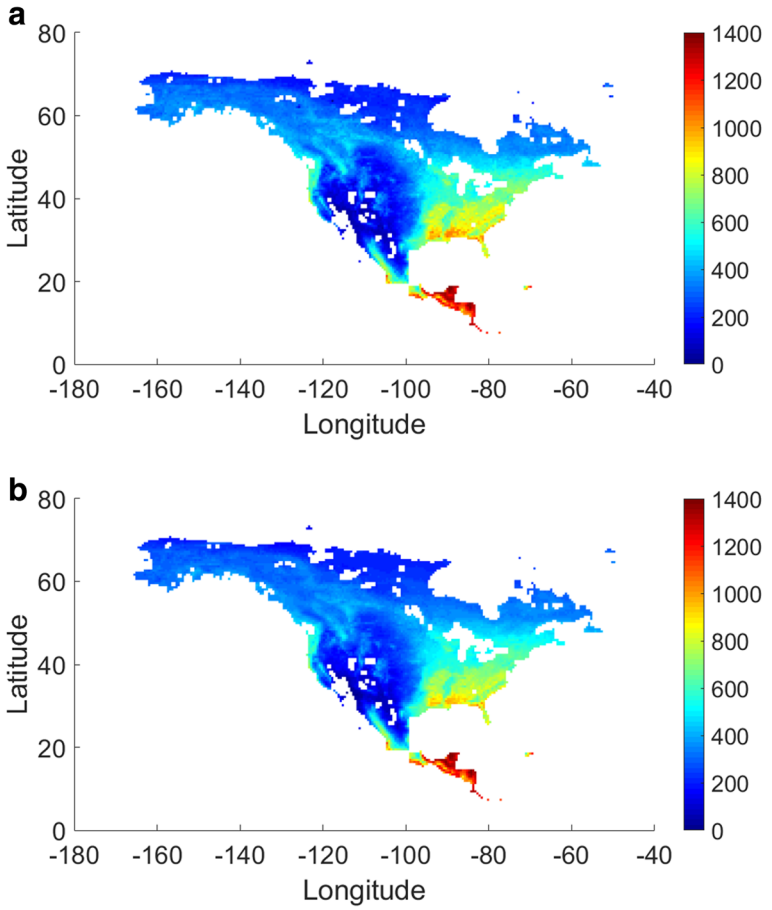

Fig. 1 Average annual ET (mm year^{-1}) from 2000 to 2010. **a** The revised TEM simulation. **b** MODIS ET product

ET simulation (AL-1) is compared with other algorithms including original TEM ET algorithm (AL-2) and the modified PM algorithm (AL-3) (Song et al. 2017). We also use site-level ET for calibration. In comparison with remote sensing product, AL-1 (R^2 = 0.82) has higher R^2 than the AL-2 ($R^2 = 0.72$) and AL-3 ($R^2 = 0.68$) for the region. Overall, the revised TEM (A1-1) better simulated ET at both site and regional levels.

3.2 Water availability in the historical period and during the twenty-first century

Water is an essential natural resource (Vörösmarty et al. 2000; Fekete et al. 2004) and also affects ecosystem carbon dynamics, especially in drought areas. Carbon uptake of ecosystems is generally thought to decrease under the water-limited environment (Hunt et al. 1996). Here, we estimate water availability for a region as the difference between precipitation and ET (P-ET).

During 2000–2010, monthly average P-ET value is 181 mm month^{-1}. An increasing trend in summer (June to August) and fall (September to November) is found (Fig. 3).

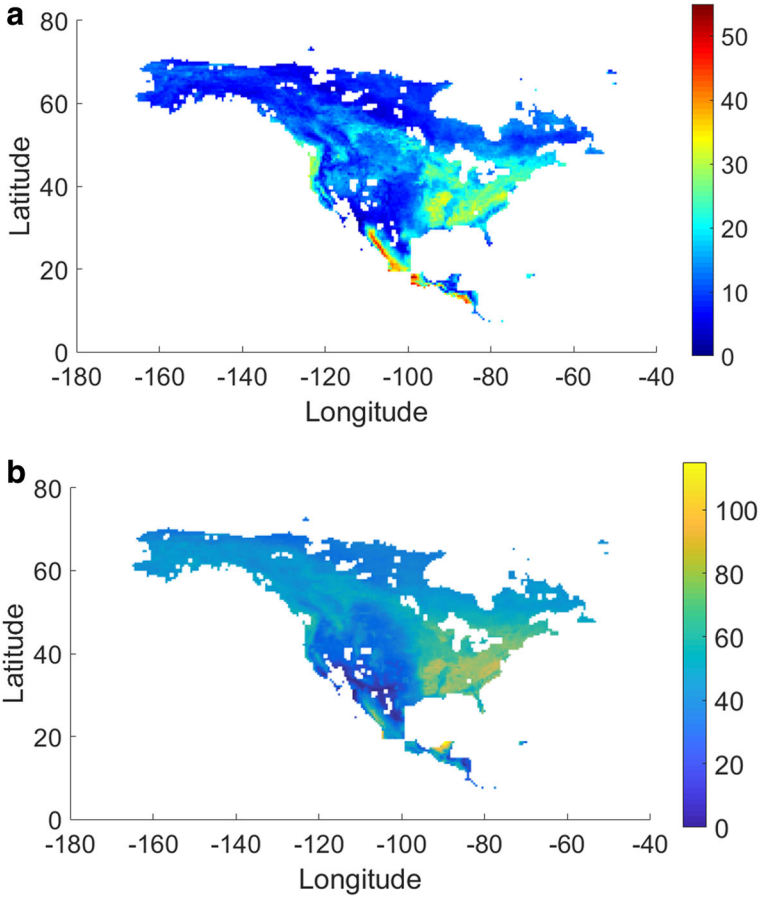

Fig. 2 Root-mean-square error (RMSE) between the revised TEM simulation and MODIS ET (mm month^{-1}) (**a**) and between the simulated ET using previous TEM and MODIS ET (mm month^{-1}) (**b**)

The seasonal average ET shows a generally decreasing trend. While the monthly P-ET value from 2000 to 2010 fluctuates significantly, it has a wetting trend. The seasonal P-ET for main subregions in North America (Alaska, Canada, the conterminous US) are extracted (Fig. 3), from which we found that the annual average P-ET in Alaska and Canada are positive, while the annual average P-ET in the conterminous US are negative. The inter-annual variability of P-ET shows an increase of 11.4 mm year^{-1} ($P < 0.1$) from 2000 to 2010. Spatially, the northwestern part of North America has a greater P-ET value (213 mm month^{-1}) than the rest of the area. Grasslands and shrublands show an increasing trend, while forests show a small decreasing trend of P-ET. When compared with SMAP data (Fig. 4), the simulated monthly P-ET value from 2000 to 2015 is positively correlated with SMAP soil moisture ($R = 0.57$).

During the twenty-first century, P-ET will decrease with increasing temperature (Fig. 5). Under an extreme climate scenario of RCP 8.5, the P-ET value decreases fast from 150 mm year^{-1} (in 2000, which is the starting point of simulation) to 80 mm year^{-1}

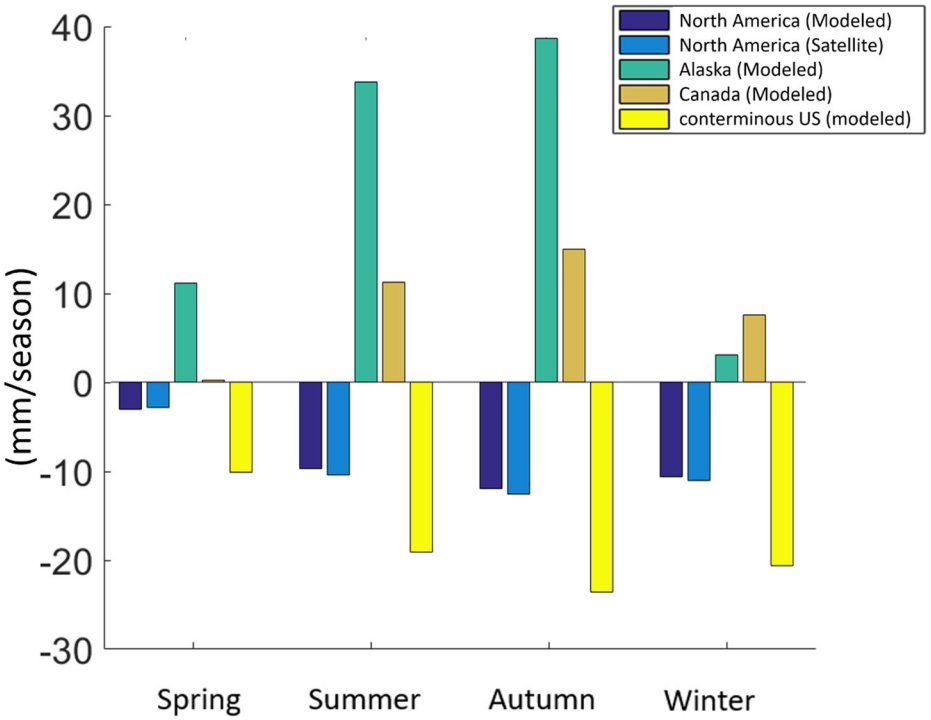

Fig. 3 Average seasonal P-ET (mm season^{-1}) for the period of 2000–2015 for subregions

at the end of the twenty-first century (Fig. 5b), indicating that the increase of temperature will reduce water availability in the future. Simulations for RCP 2.6 and 8.5 scenarios

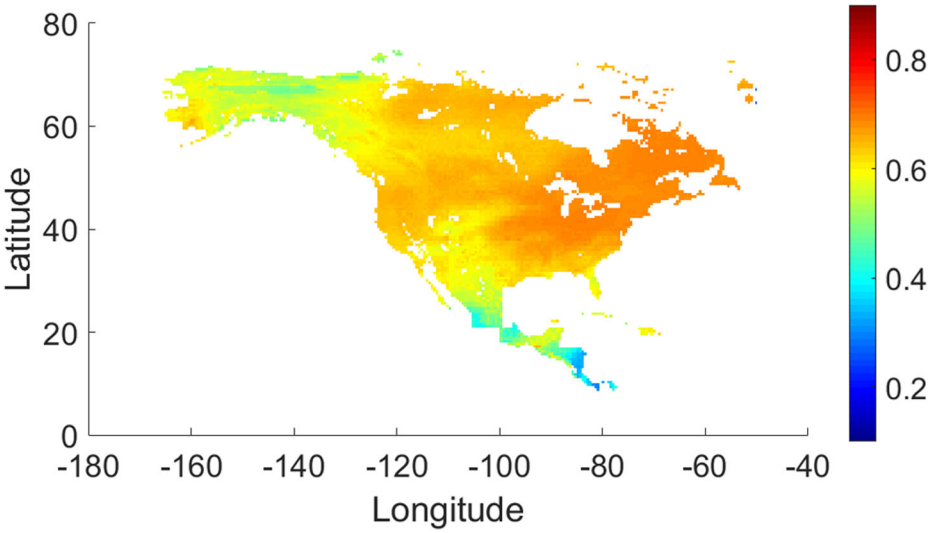

Fig. 4 Correlations between P-ET and SMAP soil moisture

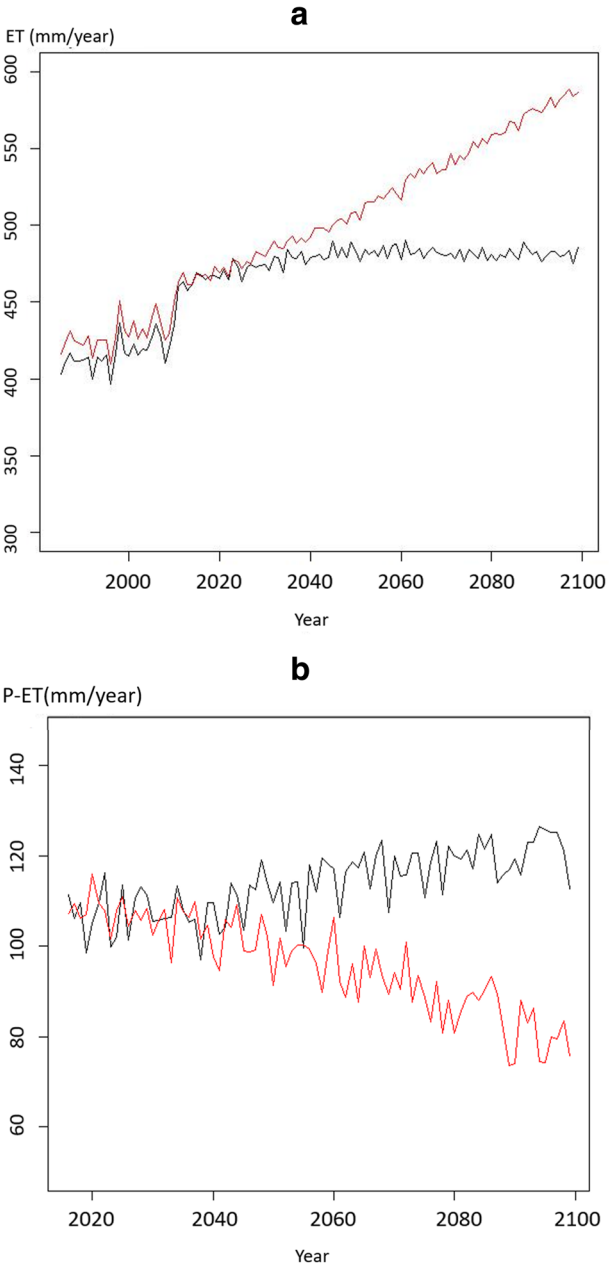

Fig. 5 **a** Simulated annual ET under the RCP 2.6 (black line) and the RCP 8.5 (red line) scenarios. **b** Simulated annual P-ET under RCP 2.6 (black line) and RCP 8.5 (red line) scenarios

show different magnitudes of ET increases with an increase of less than 10% in RCP 2.6 and 40% in RCP 8.5, respectively. These simulations suggest that North America tends to get drier with less water availability. Comparing the simulations under RCP 2.6 and

RCP 8.5 using AL-1 indicates that climate change with increasing CO_2 generally results in the lower water availability, which, in turn, affects water balance globally (Pan et al. 2015).

4 Discussion

4.1 Processes of and controls to evapotranspiration

By integrating leaf area index to ET algorithms, we manage to calibrate ET in North America in a spatially explicitly manner. To test the revised TEM, we compare it with other two algorithms. Our uncertainty analysis by varying parameters within their prior ranges is conducted with these algorithms. From 2000 to 2015, estimated regional ET in the conterminous US is 430.5 ± 10.5 mm year^{-1} (AL-1), 482.1 ± 11.2 mm year^{-1} (AL-2), and 489.7 ± 13.4 (AL-3) mm year^{-1}, respectively. The P-ET values for three algorithms are − 105.3 ± 8.7 mm year^{-1}, − 20.3 ± 11.9 mm year^{-1}, and − 126.2 ± 15.4 mm year^{-1}, respectively. AL-1 estimates a decreasing trend of ET in the twenty-first century, while the other two algorithms show an increasing trend. When comparing the three algorithms, the main difference in ET estimates is from the ET partitioning.

ET parameters including SLA, CL, and β are well calibrated. Comparing with AL-2 and AL-3, the advantage of AL-1 is that previously calibrated LAI is well integrated into the revised model with a spatially explicit set of parameters. ET simulations from AL-1 are more stable and closer to a remote sensing product (Fig. 2). In AL-2, ET is calculated separately in terms of evaporation from soil surface and transpiration from vegetation canopy. The advantage of AL-2 is the detailed estimates of different sources of ET, but it requires more parameters to be calibrated (Fig. 6a). For AL-3, evaporation is separated for different land cover types, which also requires more parameter calibration. AL-3 is more capable of simulating ET in higher-latitude areas, where evaporation from snow is better calculated (Fig. 6b).

4.2 Implications of ET change to regional water resource and the climate system

To identify ET variations in different areas in North America, we simulate P-ET for subregions including Alaska, Canada, and four regions in the conterminous US (Northwest, Northeast, Southwest, Southeast) (Fig. 3). The annual average P-ET value from 2000 to 2015 in the entire North America is negative, while Alaska and Canada have positive values and the conterminous US had negative water availability, indicating these regions have been generally dry.

Under different climate scenarios, ET variation changes water availability. Comparing with RCP 8.5, ET simulation under RCP 2.6 has lower ET, resulting in a persistent trend of P-ET in the twenty-first century, while P-ET tends to decrease under RCP 8.5. Northeast US (− 155.7 mm year^{-1}) and Northwest US (− 95.2 mm year^{-1}) have lower water availability than Southeast US (26.2 mm year^{-1}) and Southwest US (88.3 mm year^{-1}). Comparing with Southern US, Northern US in the twenty-first century have lower precipitation and higher ET, resulting in lower water availability.

Additionally, ET could influence plant productivity, affecting biomass supply and crop yield. Here, we estimated plant water use efficiency (WUE) as a ratio of plant gross primary production to ET. We find that modeled WUE and observation-based WUE at site level are

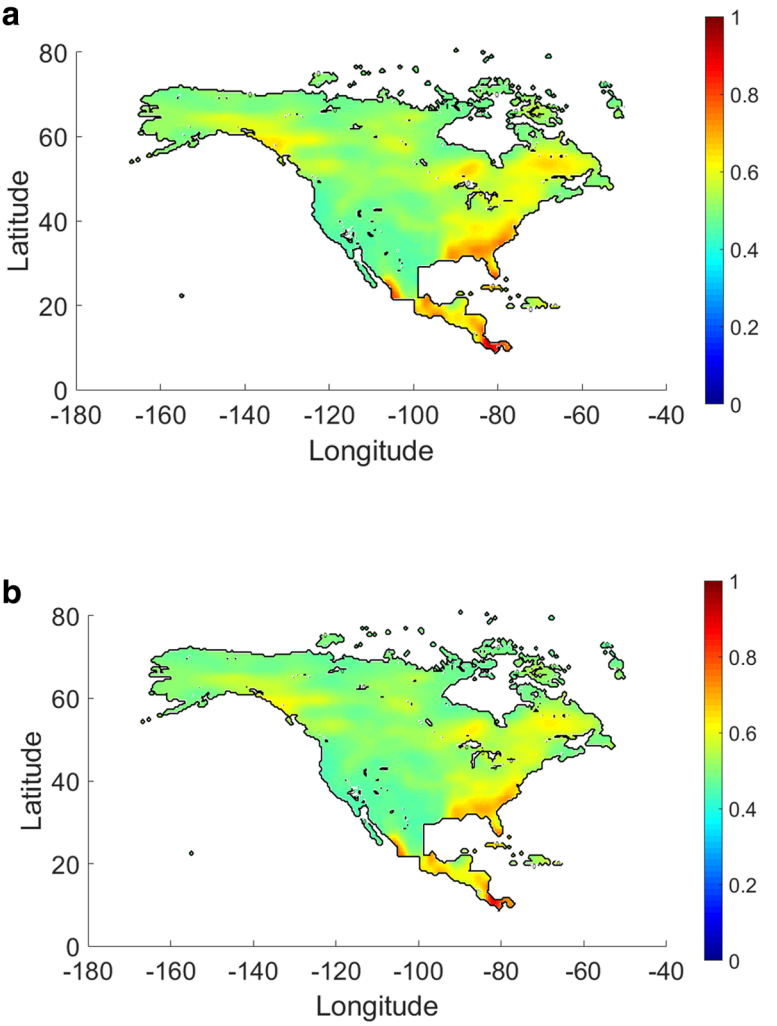

Fig. 6 Comparisons of the estimated ET between remote sensing product and different algorithms. **a** R^2 between ET from AL-2 and RS product. **b** R^2 between ET from AL-3 and RS product

well correlated ($R^2 = 0.48$), with a value of 0.68 and 0.55 for forests and grasslands, respectively. In the regions, poor correlations may result from uncertain forcing data or errors in the MODIS ET product (data not shown). Estimated WUE of forests and shrubland is higher than cropland and grasslands. Especially, the broadleaf forest has the highest WUE (3.5–4.5 g C g^{-1} H_2O). For most PFTs, WUE is higher in fall than in summer. Different PFTs have distinct WUE values. These results suggest that the ET is strongly related to plant production. Further, ET is a main source of water vapor to the atmosphere. From 2000 to 2015, the simulated ET variation (ΔET, the difference of ET between 2015 and 2000) in North America is less than 10 mm $year^{-1}$. Under the RCP 2.6 and 8.5 scenarios, ET in the twenty-first century increases by 110–155 mm $year^{-1}$. These ET or latent heat variations will affect land surface energy balance and feedback to the climate system.

5 Conclusions

This study improves ET algorithms within a process-based Terrestrial Ecosystem Model. The estimated ET with the improved model is close to MODIS monthly data. Under the RCP 2.6 and RCP 8.5 scenarios, there is an increasing trend in ET and a decreasing trend in water availability in North America. The study suggests that the region will experience a deficit of freshwater with increasing evapotranspiration in the twenty-first century. Our ET simulation under three climate change scenarios in North America suggests that the RCP 2.6 is the optimum trajectory to increase the global mean temperature by 2 °C in the twenty-first century, for preserving freshwater resources. Our case study to assess the ET impacts on water resources in North America suggests that a similar adaptation and mitigation strategy in the regional water resource use shall also be applicable for other regions in the globe. Our simulation biases may come from the energy budget calculation, including the computation of available energy, sunshine radiation, and relative sunshine duration. Specifically, the cloudiness and aerosol conditions could affect our radiation calculation, which have not been considered. Second, the limited amount of site- and regional-level observational ET data also limits our model calibration, introducing uncertainties in our regional simulations. Third, our analysis has not considered the land use change effects.

Acknowledgements This research was supported in part through computational resources provided by Information Technology at Purdue, West Lafayette, Indiana.

Funding information This research was supported by an NSF project (No. 1028291).

References

Allen RG (2000) Using the FAO-56 dual crop coefficient method over an irrigated region as part of an evapotranspiration intercomparison study. J Hydrol 229(1):27–41

Allen RG, Pereira LS, Raes D, Smith M (1998) Crop evapotranspiration—guidelines for computing crop water requirements—FAO irrigation and drainage paper 56. FAO, Rome 300(9)

Allen RG, Tasumi M, Morse A, Trezza R (2005) A Landsat-based energy balance and evapotranspiration model in Western US water rights regulation and planning. Irrig Drain Syst 19(3–4):251–268

Asrar G, Myneni RB, Li Y, Kanemasu ET (1989) Measuring and modeling spectral characteristics of a tallgrass prairie. Remote Sens Environ 27(2):143–155

Baret F, Guyot G (1991) Potentials and limits of vegetation indices for LAI and APAR assessment. Remote Sens Environ 35(2):161–173

Betts AK, Ball JH, Beljaars A, Miller MJ, Viterbo PA (1996) The land surface-atmosphere interaction: a review based on observational and global modeling perspectives. J Geophys Res Atmos 101(D3):7209–7225

Biederman JA, Scott RL, Goulden ML, Vargas R, Litvak ME, Kolb TE et al (2016) Terrestrial carbon balance in a drier world: the effects of water availability in southwestern North America. Glob Chang Biol 22(5):1867–1879

Chapin FS, McGuire AD, Randerson J, Pielke R, Baldocchi D, Hobbie SE, Roulet N, Eugster W, Kasischke E, Rastetter EB, Zimov SA, Running SW (2000) Arctic and boreal ecosystems of western North America as components of the climate system. Glob Chang Biol 6(S1):211–223

Chen M, Zhuang Q, Cook DR, Coulter R, Pekour M, Scott RL, Munger JW, Bible K (2011) Quantification of terrestrial ecosystem carbon dynamics in the conterminous United States combining a process-based biogeochemical model and MODIS and AmeriFlux data. Biogeosciences 8(2):2721–2773

Dolman AJ, De Jeu RAM (2010) Evaporation in focus. Nat Geosci 3(5):296–296

Duchemin B, Hadria R, Erraki S, Boulet G, Maisongrande P, Chehbouni A et al (2006) Monitoring wheat phenology and irrigation in Central Morocco: on the use of relationships between evapotranspiration, crops coefficients, leaf area index and remotely-sensed vegetation indices. Agric Water Manag 79(1):1–27

Edwards M, Richardson AJ (2004) Impact of climate change on marine pelagic phenology and trophic mismatch. Nature 430(7002):881–884
Fekete BM, Vörösmarty CJ, Roads JO, Willmott CJ (2004) Uncertainties in precipitation and their impacts on runoff estimates. J Clim 17(2):294–304
Fisher JB, Tu KP, Baldocchi DD (2008) Global estimates of the land–atmosphere water flux based on monthly AVHRR and ISLSCP-II data, validated at 16 FLUXNET sites. Remote Sens Environ 112(3):901–919
Hargreaves GH, Samani ZA (1985) Reference crop evapotranspiration from temperature. Appl Eng Agric 1(2): 96–99
Hargreaves GH, Allen RG (2003) History and evaluation of Hargreaves evapotranspiration equation. J Irrig Drain Eng 129(1):53–63
Hastings WK (1970) Monte Carlo sampling methods using Markov chains and their applications. Biometrika 57(1):97–109
Holland WR (1978) The role of mesoscale eddies in the general circulation of the ocean—numerical experiments using a wind-driven quasi-geostrophic model. J Phys Oceanogr 8(3):363–392
Hunt HW, Elliott ET, Detling JK, Morgan JA, Chen DX (1996) Responses of a C3 and a C4 perennial grass to elevated CO2 and temperature under different water regimes. Glob Chang Biol 2(1):35–47
Intergovernmental Panel on Climate Change (2014) Climate change 2014—impacts, adaptation and vulnerability: regional aspects. Cambridge University Press, Cambridge
Jensen ME, Haise HR (1963) Estimating evapotranspiration from solar radiation. Proc Am Soc Civ Eng, J Irrig Drain Div 89:15–41
Katul GG, Oren R, Manzoni S, Higgins C, Parlange MB (2012) Evapotranspiration: a process driving mass transport and energy exchange in the soil-plant-atmosphere-climate system. Rev Geophys 50(3)
Liang X, Lettenmaier DP, Wood EF, Burges SJ (1994) A simple hydrologically based model of land surface water and energy fluxes for general circulation models. J Geophys Res Atmos 99(D7):14415–14428
Liu Y, Zhuang Q, Chen M, Pan Z, Tchebakova N, Sokolov A et al (2013) Response of evapotranspiration and water availability to changing climate and land cover on the Mongolian Plateau during the 21st century. Glob Planet Chang 108:85–99
Liu Y, Zhuang Q, Pan Z, Miralles D, Tchebakova N, Kicklighter D, Chen J, Sirin A, He Y, Zhou G, Melillo J (2014) Response of evapotranspiration and water availability to the changing climate in northern Eurasia. Clim Chang 126(3–4):413–427
Liu Y, Zhuang Q, Miralles D, Pan Z, Kicklighter D, Zhu Q, He Y, Chen J, Tchebakova N, Sirin A, Niyogi D, Melillo J (2015) Evapotranspiration in northern Eurasia: impact of forcing uncertainties on terrestrial ecosystem model estimates. J Geophys Res Atmos 120(7):2647–2660
Lu X, Zhuang Q (2010) Evaluating evapotranspiration and water-use efficiency of terrestrial ecosystems in the conterminous United States using MODIS and AmeriFlux data. Remote Sens Environ 114(9):1924–1939
Metropolis N, Rosenbluth AW, Rosenbluth MN, Teller AH, Teller E (1953) Equation of state calculations by fast computing machines. J Chem Phys 21(6):1087–1092
Miralles DG, De Jeu RA, Gash JH, Holmes TR, Dolman AJ (2011) Magnitude and variability of land evaporation and its components at the global scale. Hydrol Earth Syst Sci 15:967–981
Monteith JL (1965) Evaporation and environment. Symp Soc Exp Biol 19(205-23):4
Mooney H, Cropper A, Reid W (2005) Confronting the human dilemma. Nature 434(7033):561–562
Mu Q, Heinsch FA, Zhao M, Running SW (2007) Development of a global evapotranspiration algorithm based on MODIS and global meteorology data. Remote Sens Environ 111(4):519–536
Mu Q, Zhao M, Running SW (2011) Improvements to a MODIS global terrestrial evapotranspiration algorithm. Remote Sens Environ 115(8):1781–1800
Mueller B, Hirschi M, Jimenez C, Ciais P, Dirmeyer PA, Dolman AJ, Miralles DG (2013) Benchmark products for land evapotranspiration: LandFlux-EVAL multi-data set synthesis. Hydrol Earth Syst Sci
Pan Y, Mcguire AD, Kicklighter DW, Melillo JM (1996) The importance of climate and soils for estimates of net primary production: a sensitivity analysis with the terrestrial ecosystem model. Glob Chang Biol 2(1):5–23
Pan S, Tian H, Dangal SR, Yang Q, Yang J, Lu C et al (2015) Responses of global terrestrial evapotranspiration to climate change and increasing atmospheric CO_2 in the 21st century. Earth's Future 3(1):15–35
Qu Y, Zhuang Q (2018) Modeling leaf area index in North America using a process-based terrestrial ecosystem model. Ecosphere 9(1)
Qu Y, Maksyutov S, & Zhuang Q (2018) An efficient method for accelerating the spin-up process for process-based biogeochemistry models. Biogeosciences 15(13)
Rasmusson EM (1968) Atmospheric water vapor transport and the water balance of North America: II. Large-scale water balance investigations. Mon Weather Rev 96(10):720–734
Riahi K, Grübler A, Nakicenovic N (2007) Scenarios of long-term socio-economic and environmental development under climate stabilization. Technol Forecast Soc Chang 74(7):887–935

Seager R, Ting M, Held I, Kushnir Y, Lu J, Vecchi G, Huang H, Harnik N, Leetmaa A, Lau N, Li C, Velez J, Naik N (2007) Model projections of an imminent transition to a more arid climate in southwestern North America. Science 316(5828):1181–1184

Sitch S, Smith B, Prentice IC, Arneth A, Bondeau A, Cramer W et al (2003) Evaluation of ecosystem dynamics, plant geography and terrestrial carbon cycling in the LPJ dynamic global vegetation model. Glob Chang Biol 9(2):161–185

Sobrino JA, Gómez M, Jiménez-Muñoz JC, Olioso A, Chehbouni G (2005) A simple algorithm to estimate evapotranspiration from DAIS data: application to the DAISEX campaigns. J Hydrol 315(1):117–125

Song L, Zhuang Q, Yin Y, Zhu X, Wu S (2017) Spatio-temporal dynamics of evapotranspiration on the Tibetan Plateau from 2000 to 2010. Environ Res Lett 12(1):014011

Sun G, Alstad K, Chen J, Chen S, Ford CR, Lin G et al (2011) A general predictive model for estimating monthly ecosystem evapotranspiration. Ecohydrology 4(2):245–255

Thornthwaite CW (1948) An approach toward a rational classification of climate. 66:(1)77. LWW

Van Vuuren DP, Den Elzen MG, Lucas PL, Eickhout B, Strengers BJ, Van Ruijven B et al (2007) Stabilizing greenhouse gas concentrations at low levels: an assessment of reduction strategies and costs. Clim Chang 81(2):119–159

Vörösmarty CJ, Federer CA, Schloss AL (1998) Potential evaporation functions compared on US watersheds: possible implications for global-scale water balance and terrestrial ecosystem modeling. J Hydrol 207(3–4): 147–169

Vörösmarty CJ, Green P, Salisbury J, Lammers RB (2000) Global water resources: vulnerability from climate change and population growth. Science 289(5477):284–288

Vörösmarty CJ, McIntyre PB, Gessner MO, Dudgeon D, Prusevich A, Green P, Glidden S, Bunn SE, Sullivan CA, Liermann CR, Davies PM (2010) Global threats to human water security and river biodiversity. Nature 467(7315):555–561

Wang K, Wang P, Li Z, Cribb M, Sparrow M (2007) A simple method to estimate actual evapotranspiration from a combination of net radiation, vegetation index, and temperature. J Geophys Res Atmos 112(D15)

Wiegand CL, Richardson AJ, Kanemasu ET (1979) Leaf area index estimates for wheat from Landsat and their implications for evapotranspiration and crop modeling. Agron J 71(2):336–342

Wilson KB, Baldocchi DD (2000) Seasonal and interannual variability of energy fluxes over a broadleaved temperate deciduous forest in North America. Agric For Meteorol 100(1):1–18

Zhang X, Friedl MA, Schaaf CB, Strahler AH, Hodges JC, Gao F et al (2003) Monitoring vegetation phenology using MODIS. Remote Sens Environ 84(3):471–475

Zhang Y, Peña-Arancibia JL, McVicar TR, Chiew FH, Vaze J, Liu C, …, Miralles DG (2016) Multi-decadal trends in global terrestrial evapotranspiration and its components. Sci Rep, 6 19124

Zhuang Q, McGuire AD, Melillo JM, Clein JS, Dargaville RJ, Kicklighter DW, Myneni RB, Dong J, Romanovsky VE, Harden J, Hobbie JE (2003) Carbon cycling in extratropical terrestrial ecosystems of the Northern Hemisphere during the 20th century: a modeling analysis of the influences of soil thermal dynamics. Tellus B 55(3):751–776

Zhuang Q, He J, Lu Y, Ji L, Xiao J, Luo T (2010) Carbon dynamics of terrestrial ecosystems on the Tibetan Plateau during the 20th century: an analysis with a process-based biogeochemical model. Glob Ecol Biogeogr 19(5):649–662

Zomer RJ, Trabucco A, Bossio DA, Verchot LV (2008) Climate change mitigation: a spatial analysis of global land suitability for clean development mechanism afforestation and reforestation. Agric Ecosyst Environ 126(1):67–80

Affiliations

Yang Qu [1,2] · Qianlai Zhuang [1,3]

[1] Department of Earth, Atmospheric, and Planetary Sciences, Purdue University, West Lafayette, IN 47907, USA

[2] Department of Natural Resources and Environmental Sciences, UIUC, Champaign, IL, USA

[3] Department of Agronomy, Purdue University, West Lafayette, IN, USA